Research Square

Preprints are preliminary reports that have not undergone peer review.
They should not be considered conclusive, used to inform clinical practice,
or referenced by the media as validated information.

Knockdown of CDCP1 Inhibits ox-LDL-Induced Phenotypic Transition and Lipid Accumulation in Vascular Smooth Muscle Cells via Downregulating the ITGB4/PI3K/AKT Pathway

Wanqiu Li
Southern University of Science and Technology Hospital
Bo Yuan
Southern University of Science and Technology Hospital
Huaihai Lu
Southern University of Science and Technology Hospital
Wei Luo
Southern University of Science and Technology Hospital
Ling Li
Southern University of Science and Technology Hospital
Hanzhao Li
Southern University of Science and Technology Hospital
Ning Zhou
Southern University of Science and Technology Hospital
Jianglang Yuan
Southern University of Science and Technology Hospital
Qianqian Dong
Second Hospital of Hebei Medical University
Xin Ji
jixin@sustech-hospital.cn

Southern University of Science and Technology Hospital

Research Article

Keywords: Atherosclerosis, Vascular smooth muscle cells, CDCP1, Phenotypic transition, ITGB4/PI3K/AKT pathway, Lipid accumulation

Posted Date: September 10th, 2026

DOI: https://doi.org/10.21203/rs.3.rs-10795450/v1

License: This work is licensed under a Creative Commons Attribution 4.0 International License.
Read Full License

Additional Declarations: No competing interests reported.

Abstract

The transition of vascular smooth muscle cells (VSMCs) toward a macrophage-like phenotype is a key event driving atherosclerosis (AS) progression. CUB domain-containing protein 1 (CDCP1) is involved in cellular remodeling and signal transduction, associated with cardiovascular pathology, but its function in AS is still unclear. Here, we investigated whether CDCP1 regulates VSMC macrophage-like phenotypic transition and lipid accumulation during AS progression. Differential expression analysis of the human vascular transcriptomic datasets GSE43292 and GSE28829 identified CDCP1 as a commonly upregulated gene in atherosclerotic plaque tissues. Immunohistochemical staining further confirmed increased CDCP1 expression in aortic arch plaques from high-fat diet-fed ApoE$^{-/-}$ mice. In primary mouse VSMCs, siRNA-mediated CDCP1 knockdown suppressed ox-LDL-induced macrophage-like phenotypic transition, as shown by Western blot and immunofluorescence analysis. Oil Red O staining, BODIPY 493/503 staining and DiI-ox-LDL uptake assays further showed that CDCP1 silencing reduced lipid accumulation, lipid droplet formation and ox-LDL uptake. RNA sequencing followed by KEGG enrichment analysis demonstrated that CDCP1 knockdown modulated the PI3K/AKT pathway, with ITGB4 identified as a markedly downregulated upstream molecule. Mechanistically, CDCP1 silencing decreased ITGB4 expression mainly by reducing ITGB4 mRNA stability, thereby inhibiting PI3K/AKT pathway activation and limiting VSMC macrophage-like transition and lipid accumulation. Collectively, CDCP1 emerges as a key mediator of VSMC pathological remodeling and lipid loading, highlighting its potential as a molecular target for AS intervention.

1. Introduction

Atherosclerosis (AS) is a persistent inflammation-related vascular disorder affecting large and medium arteries throughout the body, forming the main pathological foundation for cardiovascular and cerebrovascular illnesses[1]. Globally, AS-related diseases contribute significantly to disability and mortality, posing a substantial burden on public health[2]. Current clinical strategies for the prevention and treatment of AS mainly include lipid-lowering therapy, antiplatelet treatment, and interventions aimed at improving vascular function[3]. Although these approaches can delay disease progression and reduce cardiovascular events to some extent, they do not fully reverse pathological vascular remodeling[4]. Consequently, elucidating the molecular mechanisms involved in AS pathogenesis and finding safe, effective therapeutic targets are of critical clinical and scientific importance.

As the predominant cells in the vascular media, vascular smooth muscle cells (VSMCs) possess distinctive phenotypic plasticity and play a critical role in maintaining vasomotor function[5]. In normal physiological states, VSMCs are predominantly differentiated into a contractile phenotype with minimal proliferative and migratory capacities, primarily responsible for regulating vascular tone and maintaining vessel wall structural integrity[6]. Nevertheless, upon stimulation by pathological factors such as oxidized low-density lipoprotein (ox-LDL) accumulation, abnormal lipid buildup, and chronic inflammation, VSMCs transition from a contractile to a macrophage-like phenotype[7]. These transitioned VSMCs not only lose their inherent contractile function but also acquire robust capacities

for proliferation, migration, lipid phagocytosis, and pro-inflammatory secretion, thereby driving the progression of early fatty streaks into mature vulnerable plaques, a critical link in AS progression and plaque destabilization[8]. Recent single-cell sequencing and lineage-tracing studies have further demonstrated that a substantial proportion of macrophage-like cells within atherosclerotic plaques originate from phenotypically transformed VSMCs[9]. Thus, clarifying the regulatory mechanisms governing the macrophage-like transition of VSMCs and identifying key molecules capable of interrupting this pathological cascade may provide an important strategy for limiting AS progression.

CUB domain-containing protein 1 (CDCP1), a type I transmembrane glycoprotein, is involved in several biological processes like cell proliferation, membrane receptor trafficking, and post-translational modification regulation. It is aberrantly overexpressed in various malignant tumors, mediating tumor invasion and metastasis[10, 11]. In recent years, the biological functions of CDCP1 in the cardiovascular system have garnered increasing attention. One study demonstrated that patients with ST-segment elevation myocardial infarction possess notably increased circulating levels of CDCP1 expression[12]. Another study indicated that the knockdown of CDCP1 significantly suppresses PDGF-BB-induced VSMC proliferation and migration through modulating the endocytosis and degradation of PDGFRβ[13]. Nevertheless, whether CDCP1 participates in the ox-LDL-induced phenotypic transition of VSMCs and contributes to AS progression remains unclear.

Building upon these findings, this study established a high-fat diet (HFD)-induced AS mouse model and an ox-LDL-stimulated VSMC phenotypic transition model to systematically investigate the function of CDCP1 in AS progression. Specifically, we aimed to clarify whether CDCP1 regulates the macrophage-like transition of VSMCs and examine the underlying molecular cascades. These results may uncover new aspects of AS pathogenesis and indicate potential intervention targets.

2. Materials and Methods

2.1 Main Reagents

ox-LDL, cycloheximide (CHX), and actinomycin D (Sigma, USA); DMEM medium (Gibco, USA); fetal bovine serum (FBS, Hyclone, USA); Cholesterol (TC), Triglycerides (TG), Low-density lipoprotein cholesterol (LDL-C), and High-density lipoprotein cholesterol (HDL-C) assay kits (Nanjing Jiancheng Bioengineering Institute, China); Oil Red O (ORO) and hematoxylin-eosin (HE) staining kits, and CCK-8 assay kit (Beyotime, China); Lipofectamine 3000 (Invitrogen, USA); BODIPY 493/503 fluorescent dye and Dil-ox-LDL (Invitrogen, USA); RNA extraction, reverse transcription, and real-time quantitative PCR (qPCR) kit (Tiangen, China); IGF-1 (MCE, USA); dual-luciferase reporter assay kit (Promega, USA). All plasmids were synthesized by Genechem (China).

2.2 Bioinformatics Analysis

The GEO database was used to obtain the human atherosclerotic plaque tissue transcriptome datasets GSE43292 and GSE28829. After probe annotation and data normalization according to the

corresponding platform annotation files, the 'limma' package in R was utilized to detect differentially expressed genes (DEGs). The criteria for screening were set as $|\log_2$ fold change (FC)$| > 1$ and $P < 0.05$. The intersection of DEGs from the two datasets was then obtained to identify candidate genes consistently upregulated in atherosclerotic plaque tissues.

2.3 Experimental Animals

Twenty male ApoE$^{-/-}$ mice (eight weeks old, 20–22 g body weight) were acquired from Beijing Weitong Lihua Experimental Animal Technology Co., Ltd. (China). The animals were kept in SPF conditions. Environmental parameters included 55 ± 5% relative humidity, 22 ± 2°C ambient temperature, and a 12h dark/light photoperiod, alongside ad libitum provision of water and standard chow. After acclimating for a week, mice were assigned to two groups (n = 10): the normal diet (ND) group, receiving standard maintenance chow, and the HFD group, which was continuously provided with a HFD for 12 weeks. After the experiment was completed, the mice were euthanized by administering an intraperitoneal overdose of sodium pentobarbital, and blood and aortic tissues gathered for further study. This animal study protocol was approved by the Animal Ethics Committee ofGuangdong Medical Experimental Animal Center (number D202403-51).

2.4 Measurement of Serum Lipid Levels

Collected blood samples were allowed to stand at 4°C for 30 min, then centrifuged at 3000 rpm for 10 min to separate the serum. The serum concentrations of TC, TG, HDL-C, and LDL-C were determined following the manufacturers' guidelines for the respective assay kits.

2.5 Histopathological Analysis

ORO staining was performed to evaluate lipid deposition in both the full-length aorta and aortic arch sections. For *en face* ORO staining, the intact mouse aorta was carefully isolated, the vessel was then opened lengthwise and flattened. After pretreatment with 60% isopropanol, the samples were immersed in 0.5% ORO solution and stained for 1 h. Subsequently, the samples were differentiated with 60% isopropanol, images were obtained with the light microscope (Olympus, Japan). For ORO staining of aortic arch sections, frozen sections of aortic arch were sliced to 5 μm and equilibrated to room temperature. The sections were pretreated with 60% isopropanol, then exposed to the ORO working solution for 30 min. After using isopropanol for differentiation to clear nonspecific staining, the sections underwent counterstaining with hematoxylin, mounted, and observed with the light microscope.

For HE staining of the aortic arch, mouse aortic arch tissues were immersed in 4% paraformaldehyde for 24 h. After the typical steps for dehydration, clearing, and paraffin infiltration, 5-μm-thick sections were prepared. The paraffin-embedded slices were deparaffinized, rehydrated, and subjected to HE staining following the provided kit instructions. Finally, the stained sections underwent dehydration, clearing, and mounting prior to microscopic imaging.

2.6 Immunohistochemical Staining

Aortic arch paraffin sections were deparaffinized, rehydrated, and incubated with 3% hydrogen peroxide for 15 minutes. Following antigen retrieval, sections were blocked using 5% goat serum for 1 h at room temperature and exposed to the CDCP1 primary antibody throughout the night at 4°C. The following day, the sections were washed with PBS and then incubated with a secondary antibody for 1 h. After DAB color development, the sections were counterstained with hematoxylin, dehydrated, and mounted. A light microscope was used to image the samples.

2.7 Primary Culture of Mouse Vascular Smooth Muscle Cells (mVSMCs)

According to previous methods, primary mVSMCs were extracted from mouse aortas [14]. In brief, mice received an intraperitoneal injection of 1% sodium pentobarbital for anesthesia. The thoracic and abdominal aortas were isolated under sterile conditions, and the surrounding adipose and connective tissues were carefully removed. After rinsing the vessels with sterile PBS, the aortas were longitudinally opened in DMEM. The tissues were sliced into roughly 1 mm^3 fragments, uniformly transferred to a cell culture dish and incubated at 37°C with 5% CO_2 for 4 h to facilitate attachment. Subsequently, DMEM containing 20% FBS and 1% penicillin/streptomycin (1% P/S) was gently introduced, and the explants were maintained for another 5 days. Culture media were refreshed every 2–3 days, and cells that migrated from the tissue fragments were passaged upon reaching 80%–90% confluence. Cell purity was assessed by detecting SMA expression.

2.8 Cell Culture and Treatment

mVSMCs incubated at 37°C in DMEM medium with 10% FBS and 1% P/S under 5% CO_2 conditions. To construct the VSMCs phenotypic transition model, cells were subjected to different ox-LDL concentrations for 24 h. The optimal ox-LDL concentration for subsequent experiments was identified through the CCK-8 assay.

For transfection, cells were cultured in 6-well plates. Upon reaching 60%–70% confluence, si-NC, si-CDCP1, empty vector, or ITGB4 overexpression plasmids were introduced into the cells following the Lipofectamine 3000 manufacturer's protocol. Cells were collected 48 h after transfection for subsequent experiments. To activate the PI3K/AKT pathway, cells t with si-CDCP1 transfection were exposed to IGF-1 (100 ng/mL) for 24 h.

2.9 CCK-8 Assay

In the phase of logarithmic growth, mVSMCs were cultured overnight in 96-well plates with 5×10^3 cells per well. Afterward, they were treated with various ox-LDL concentrations for 24 h. A 10-μL volume of CCK-8 solution was introduced to each well, then incubated at 37°C for 2 h. Cell viability was determined by measuring absorbance at 450 nm with microplate reader (Thermo Fisher, USA).

2.10 Cellular ORO Staining

Following the completion of cell treatments, the medium was removed. The cells were exposed to 4% paraformaldehyde for 15 min, followed by a 1-minute incubation with 60% isopropanol, and then treated with the ORO working solution for 20 min. To remove background color, 60% isopropanol was utilized for differentiation. After staining the mVSMCs with hematoxylin for 1 min, they were photographed using a light microscope.

2.11 BODIPY 493/503 Lipid Droplet Staining

Following the experimental treatments, the initial medium was removed and substituted with a serum-free medium containing 1 μg/mL BODIPY 493/503 and 5 μg/mL Hoechst 33342. The mVSMCs underwent a 15-minute incubation at 37°C in darkness. The dye solution was eliminated, and the cells were washed with PBS to eliminate unbound probes. After mounting with an anti-fluorescence quenching reagent, lipid droplet formation was observed using a fluorescence microscope (Olympus, Japan).

2.12 Dil-ox-LDL Lipid Uptake Assay

Following cell treatments, the medium was substituted with a serum-free medium that included 40 μg/mL Dil-ox-LDL, and the mVSMCs were maintained at 37°C, 5% CO_2 for 6 h. After rinsing the mVSMCs with PBS to eliminate uningested Dil-ox-LDL, they underwent fixation with 4% paraformaldehyde for 15 min. The cells were then stained with DAPI for 10 min, mounted with an anti-fade reagent, and imaged under a fluorescence microscope.

2.13 RNA Sequencing (RNA-seq) and Bioinformatics Analysis

RNA-seq was conducted on mVSMCs from si-NC and si-CDCP1 groups. Following extraction and quality assessment, total RNA samples that met the criteria were depleted of rRNA, fragmented, and converted into double-stranded cDNA through reverse transcription. Sequencing libraries were prepared and sequenced on an Illumina HiSeq platform using a paired-end approach. Adapters and low-quality sequences were filtered out from the raw reads to produce clean reads, which were then aligned to the mouse reference genome using HISAT2. FeatureCounts was used to quantify gene expression, and DESeq2 was employed to identify differentially expressed genes (DEGs) with criteria of $|\log_2 FC| > 1$ and $P < 0.05$. GO and KEGG enrichment analyses were conducted via clusterProfiler ($P < 0.05$).

2.14 qPCR

The RNA extraction kit was used to extract total RNA. After determination of RNA concentration and purity, cDNA synthesis was carried out with a reverse transcription kit. qPCR was conducted using cDNA as the template following the manufacturer's kit protocols. Gene expression levels were normalized to β-actin, and relative gene expression was quantified using the $2^{-\Delta\Delta Ct}$ method. The primer sequences used were as follows: ITGB4, forward 5'-ACACAAGCTCCAGCAGACGAAG-3', reverse 5'-TCCACCTGCTTCTCTGTCAGCT-3'. β-actin, forward 5'-CATTGCTGACAGGATGCAGAAGG-3', reverse 5'-TGCTGGAAGGTGGACAGTGAGG-3'.

2.15 Dual Luciferase Reporter Assay

By cloning the ITGB4 promoter region into the pGL3-Basic vector, the pGL3-ITGB4 recombinant plasmid was constructed. mVSMCs were grown in 96-well plates, and when they reached 60%–70% confluence, the recombinant plasmid and internal reference plasmid were co-transfected with si-NC or si-CDCP1, respectively. The medium was removed 48 hours after transfection, and cells were lysed according to the dual-luciferase assay kit instructions. Following supernatant collection, the luminescence of firefly and Renilla luciferase was quantified sequentially with a microplate reader. The relative luciferase activity was determined by normalizing to Renilla luciferase activity.

2.16 Actinomycin D Assay

mVSMCs were placed in 6-well plates and transfected with si-NC or si-CDCP1. Actinomycin D was introduced to the medium 48 h later at 5 μg/mL to inhibit *de novo* mRNA synthesis. Cells were collected at 0, 2, 4, and 8 h after actinomycin D was introduced. RNA was isolated, transcribed into cDNA, and ITGB4 mRNA expression was detected by qPCR. An mRNA degradation curve was plotted using the mRNA expression level at 0 h as the baseline.

2.17 CHX Chase Assay

mVSMCs were seeded in 6-well plates and transfected with si-NC or si-CDCP1. At 48 h post-transfection, CHX was introduced into the medium at 50 μg/mL to inhibit protein translation. At 0, 3, 6, and 9 hours post-CHX addition, cells were harvested. Total cellular protein was extracted using RIPA lysis buffer, and ITGB4 protein expression at each time point was detected by Western blot. A protein degradation curve was plotted using the expression level at 0 h as the baseline.

2.18 Immunofluorescence Staining

For tissue detection, 5 μm-thick paraffin sections of aortic arches were rehydrated and underwent antigen retrieval. For cellular samples, treated mVSMCs were seeded on sterile coverslips. All cell and tissue samples were incubated using 4% paraformaldehyde for 15 min, then permeabilized with 0.2% Triton X-100 for 10 min and blocked with 5% BSA for 1 h. Samples underwent overnight incubation with primary antibodies at 4°C, followed by 1 h incubation with fluorescent secondary antibodies after PBS washing. DAPI was used to counterstain the nuclei for 10 minutes, specimens were then mounted with anti-fade medium and visualized with a confocal laser scanning microscope (Olympus, Japan).

2.19 Western Blot

RIPA buffer was employed to extract total protein from cells or tissues. After being quantified, samples combined with loading buffer were boiled for denaturation, and equal protein quantities were separated using SDS-PAGE before wet transfer to PVDF membranes. The membranes were blocked using 5% skim milk for an hour, incubated with primary antibodies overnight at 4°C, washed with TBST, and then exposed to secondary antibodies for an hour. ECL reagent was used to visualize protein bands, and band gray values were quantified with Image J. Antibody details are provided in Table 1.

Table 1
Antibody information

Antibody	Manufacturer	Cat.No.	Dilution factor
CDCP1	Proteintech	12754-1-AP	1:1000
SMA	CST	19245	1:1000
CD68	CST	97778	1:1000
MMP9	Proteintech	82854-8-RR	1:5000
ITGB4	Abcam	ab182120	1:1000
p-PI3K	CST	4228	1:1000
PI3K	CST	4257	1:1000
p-AKT	CST	9271	1:1000
AKT	CST	9272	1:1000
β-actin	CST	4970	1:2000

2.20 Statistical Analysis

GraphPad Prism 9.0 was employed for statistical analysis, and the data are presented as mean±standard deviation ($\bar{x}\pm s$). To compare two groups, an unpaired Student's t-test was employed, whereas one-way ANOVA was used for multiple group comparisons. Statistical significance was set at $P < 0.05$.

3. Results

3.1 CDCP1 expression is upregulated in AS aortic arch tissues of HFD-fed ApoE$^{-/-}$ mice

To identify key molecules that contribute to AS progression, we conducted differential expression analysis using human plaque tissue transcriptome datasets GSE43292 and GSE28829. The GSE43292 dataset comprises AS plaque tissues and relatively normal adjacent intimal tissues, whereas GSE28829 includes early and advanced atherosclerotic plaque tissues. Through differential expression analysis, we identified 216 differentially expressed genes (DEGs) in the GSE28829 dataset and 90 DEGs in the GSE432929 dataset (Fig. 1A). Further intersection analysis identified CDCP1 as one of the commonly upregulated DEGs shared by both datasets (Fig. 1B).

To validate these bioinformatics findings, we developed an AS mouse model by providing ApoE$^{-/-}$ mice with an HFD. The mice were euthanized after 12 weeks of consistent feeding, and their serum and aortic tissues were gathered. Further biochemical assessments revealed that the HFD group had elevated serum levels of TC, TG, and LDL-C, whereas the HDL-C level was notably lower than in the ND group

(Fig. 1C). Additionally, ORO staining demonstrated that the aortic plaque area was considerably larger in the HFD group compared to the ND group, suggesting that the high-fat diet induced substantial aortic lipid deposition and plaque formation (Fig. 1D). Consistently, HE and ORO staining of the aortic arch revealed pronounced pathological changes and plaque formation in the HFD group, along with a notable rise in local lipid deposition (Fig. 1E-F). Furthermore, immunohistochemical analysis showed that the HFD group exhibited a notably higher level of CDCP1-positive staining in the aortic arch plaques than the ND group (Fig. 1G). Collectively, these results demonstrate that CDCP1 is prominently expressed in both human AS aortic arch tissues and HFD-fed ApoE$^{-/-}$ mouse aortic arch tissues, suggesting that CDCP1 may be closely associated with AS plaque formation and disease progression.

3.2 ox-LDL induces macrophage-like phenotypic transition in mVSMCs and upregulates CDCP1 expression

The phenotypic transition of mVSMCs into macrophage-like cells is a critical pathological process in AS progression[15]. To investigate whether CDCP1 is involved in this process, we initially stimulated mVSMCs with ox-LDL to mimic the AS microenvironment *in vitro*. To determine the optimal ox-LDL concentration, CCK-8 assay was performed to evaluate the viability of mVSMCs exposed to varying ox-LDL concentrations for 24 h. The results showed that mVSMC viability progressively declined as ox-LDL concentrations increased. Notably, 200 μg/mL ox-LDL significantly lowered cell viability, while 100 μg/mL ox-LDL did not have a significant impact (Fig. 2A). Therefore, 100 μg/mL ox-LDL for 24 h was used for further experiments. To assess phenotypic transition, Western blot was performed for the mVSMC contractile marker SMA and macrophage phenotypic markers CD68 and MMP9. The findings revealed that ox-LDL notably reduced SMA expression and increased the expression of CD68 and MMP9 (Fig. 2B). Consistently, immunofluorescence analysis indicated a marked reduction in SMA expression and a notable elevation in CD68 expression in mVSMCs exposed to ox-LDL (Fig. 2C). Furthermore, we observed that ox-LDL markedly upregulated CDCP1 expression in mVSMCs (Fig. 2D). Collectively, these findings imply that ox-LDL prompts mVSMCs to undergo a phenotypic change into macrophage-like cells and upregulates CDCP1 expression, suggesting that CDCP1 may participate in ox-LDL-mediated mVSMC phenotypic transition.

3.3 CDCP1 knockdown inhibits ox-LDL-induced macrophage-like phenotypic transition and lipid accumulation in mVSMCs

To further determine the function of CDCP1 in ox-LDL-induced mVSMC phenotypic transition, we transfected mVSMCs with siRNA targeting CDCP1 to knock down its expression. Western blot analysis showed a significant decrease in CDCP1 protein expression in the si-CDCP1 group compared to the si-NC group, suggesting a high knockdown efficiency (Fig. 3A). Furthermore, with ox-LDL stimulation, the suppression of CDCP1 resulted in a significant increase in SMA expression and a notable decrease in the protein levels of CD68, MMP9, and CDCP1 in mVSMCs. (Fig. 3A). Immunofluorescence staining

further corroborated the Western blot results (Fig. 3B). Subsequently, we evaluated how CDCP1 influences lipid buildup in mVSMCs. ORO staining showed that ox-LDL treatment substantially increased intracellular lipid accumulation, while CDCP1 knockdown markedly decreased this accumulation (Fig. 3C). Consistently, BODIPY 493/503 staining showed massive lipid droplet formation in mVSMCs within the si-NC + ox-LDL group, notably diminished by CDCP1 knockdown (Fig. 3D). Additionally, the Dil-ox-LDL uptake assay demonstrated that ox-LDL stimulation greatly increased the uptake capacity of mVSMCs for Dil-ox-LDL. However, following CDCP1 knockdown, the intracellular Dil-ox-LDL fluorescence signal was markedly diminished (Fig. 3E). Collectively, these findings imply that CDCP1 knockdown inhibits ox-LDL- triggered macrophage-like phenotypic transition and reduces intracellular lipid accumulation in mVSMCs.

3.4 CDCP1 knockdown downregulates the ITGB4/PI3K/AKT pathway

To explore the molecular mechanisms through which CDCP1 regulates the macrophage-like phenotypic transition of mVSMCs, we extracted RNA from mVSMCs transfected with si-NC or si-CDCP1 and performed RNA-seq. Through differential expression analysis, we identified 20 DEGs between the two groups (Fig. 4A). Subsequent KEGG pathway enrichment analysis of these DEGs indicated a notable enrichment in the PI3K/AKT pathway, implying that CDCP1 may contribute to the pathological phenotypic transition of mVSMCs by modulating PI3K/AKT signaling (Fig. 4B). Given that ITGB4 is a crucial upstream regulator of the PI3K/AKT signaling pathway, we further analyzed the changes in ITGB4 expression following CDCP1 knockdown. qPCR results showed that ITGB4 expression was notably decreased following CDCP1 knockdown group (Fig. 4C). Subsequently, we used immunofluorescence to detect proteins associated with the ITGB4/PI3K/AKT pathway in mouse aortic arch tissues. The findings revealed that the expression of ITGB4, p-PI3K, and p-AKT were significantly upregulated in the aortic arch tissues of HFD-fed mice compared to the ND group, suggesting the ITGB4/PI3K/AKT pathway is activated in AS aortic arch tissues (Fig. 4D).

Next, we further explored the regulatory effect of CDCP1 on the ITGB4/PI3K/AKT signaling pathway *in vitro*. Western blot analysis demonstrated that ox-LDL stimulation significantly upregulated ITGB4, p-PI3K, and p-AKT expression in mVSMCs. Conversely, CDCP1 knockdown markedly attenuated the ox-LDL-induced upregulation of ITGB4, p-PI3K, and p-AKT. Notably, the overall protein levels of PI3K and AKT remained unchanged across the groups (Fig. 4E). Collectively, these findings demonstrate that CDCP1 knockdown suppresses ox-LDL-mediated activation of the ITGB4/PI3K/AKT pathway.

3.5 CDCP1 knockdown reduces ITGB4 expression by decreasing ITGB4 mRNA stability

We previously demonstrated that CDCP1 knockdown decreased ITGB4 mRNA levels in mVSMCs (Fig. 4C). Next, we evaluated the effect of CDCP1 knockdown on ITGB4 protein expression. Consistent

with the qPCR results, CDCP1 knockdown significantly reduced ITGB4 protein levels in mVSMCs, suggesting that CDCP1 may regulate ITGB4 expression by affecting ITGB4 mRNA abundance (Fig. 5A). Since mRNA abundance is determined by both transcriptional activity and mRNA stability, we next sought to determine how CDCP1 regulates ITGB4 expression. The results of dual-luciferase reporter assay showed no significant change in ITGB4 promoter activity following CDCP1 knockdown, indicating that CDCP1-mediated regulation of ITGB4 expression is independent of alterations in promoter transcriptional activity (Fig. 5B). Next, we used actinomycin D to inhibit new mRNA synthesis in cells and assessed ITGB4 mRNA degradation at various time intervals. Results indicated that ITGB4 mRNA degradation was significantly accelerated and its half-life was greatly shortened in the si-CDCP1 group relative to the si-NC group, demonstrating that CDCP1 knockdown destabilizes ITGB4 mRNA (Fig. 5C). Notably, CHX chase assay results showed that the degradation rate of ITGB4 protein remained unaltered following CDCP1 knockdown, implying that CDCP1 knockdown does not significantly affect ITGB4 protein stability (Fig. 5D). In summary, these findings demonstrate that CDCP1 knockdown downregulates ITGB4 expression primarily by reducing ITGB4 mRNA stability, rather than by inhibiting ITGB4 transcription or promoting ITGB4 protein degradation.

3.6 CDCP1 promotes macrophage-like phenotypic transition and lipid accumulation in mVSMCs through the ITGB4/PI3K/AKT pathway

To further confirm whether the ITGB4/PI3K/AKT pathway is involved in CDCP1-mediated mVSMC phenotypic transition and lipid accumulation, we performed rescue experiments. Following CDCP1 knockdown and ox-LDL stimulation, we either overexpressed ITGB4 or treated the cells with the PI3K/AKT pathway activator IGF-1. Western blot analysis showed that both ITGB4 overexpression and IGF-1 treatment significantly increased the protein expression levels of p-PI3K and p-AKT in mVSMCs. However, ITGB4 overexpression also significantly upregulated ITGB4 protein expression, whereas IGF-1 had no significant effect on ITGB4 expression (Fig. 6A). Subsequently, we evaluated the phenotypic transition of mVSMCs under different treatment conditions. Western blot results revealed that both ITGB4 overexpression and IGF-1 treatment markedly downregulated SMA expression and upregulated CD68 and MMP9 expression (Fig. 6B). Immunofluorescence findings were consistent with the Western blot results (Fig. 6C). Additionally, ORO staining demonstrated that both ITGB4 overexpression and IGF-1 treatment significantly enhanced lipid accumulation in mVSMCs (Fig. 6D). Consistently, BODIPY 493/503 staining indicated that both treatments markedly promoted intracellular lipid droplet formation in mVSMCs (Fig. 6E). Furthermore, the Dil-ox-LDL uptake assay revealed that both ITGB4 overexpression and IGF-1 treatment distinctly augmented the ox-LDL uptake capacity of mVSMCs (Fig. 6F). Collectively, these results demonstrate that CDCP1 promotes the macrophage-like phenotypic transition and lipid accumulation in mVSMCs through modulating the ITGB4/PI3K/AKT signaling pathway.

4. Discussion

AS represents a chronic vascular disorder mediated by multiple factors, with a pathogenesis that encompasses various pathological processes, including lipid metabolism issues, chronic inflammation, and abnormal remodeling of vascular cells[16] Although statins and antiplatelet drugs exhibit efficacy in regulating blood lipids and delaying plaque formation, long-term administration frequently induces adverse effects, such as hepatic dysfunction and myalgia, and some patients may develop drug tolerance. More critically, these pharmacological interventions fail to repair established structural and functional damage to the vascular wall, leaving patients with a substantial residual cardiovascular risk[17]. Therefore, further elucidation of the molecular mechanisms underlying AS progression and the discovery of new intervention targets remain important for improving therapeutic outcomes.

The current research identified CDCP1 as a gene commonly upregulated in human atherosclerotic plaque tissues based on the analysis of the GSE43292 and GSE28829 datasets. Consistently, CDCP1-positive staining was markedly increased in aortic arch tissues of AS mice, suggesting that CDCP1 may participate in AS progression. CDCP1, a type I transmembrane glycoprotein featuring CUB domains, is involved in biological processes like cell survival, migration, invasion, and intracellular signal transduction [18, 19]. Aberrant CDCP1 expression has been widely reported in malignant tumors, where it contributes to tumor progression and metastatic behavior. More recently, the role of CDCP1 in cardiovascular diseases has attracted increasing attention. For example, previous research has revealed that CDCP1 is involved in myocardial remodeling, mechanistic evidence suggests that CDCP1 could regulate fibroblast activation and myocardial fibrosis through AKT-related signaling pathways [20].

VSMC phenotypic transition is a central pathological event in AS progression. Under normal conditions, VSMCs exhibit a contractile phenotype, contributing to vascular tone and vessel wall integrity. In reaction to pathological factors like ox-LDL, inflammation mediators, and lipid accumulation, VSMCs can lose contractile marker expression and acquire macrophage-like or foam cell-like characteristics. This process is accompanied by enhanced lipid uptake, inflammatory activation, extracellular matrix remodeling, and plaque destabilization, thereby linking lipid deposition to plaque progression [21]. Previous studies have indicated that targeting VSMC phenotypic transition may be an effective strategy for limiting AS development. For example, miR-145 micelles suppress AS plaque formation by restoring contractile marker expression in synthetic VSMCs [22], whereas tryptanthrin delays AS progression by inhibiting VSMC phenotypic transition through the AMPK/ACC pathway [23].

This research found that ox-LDL stimulation induced a macrophage-like phenotypic transition in mVSMCs, indicate by reduced SMA expression and elevated levels of CD68 and MMP9. Notably, CDCP1 expression was elevated after ox-LDL treatment, indicating that CDCP1 might play a part in the pathological reprogramming of mVSMCs triggered by ox-LDL Further functional experiments showed that CDCP1 knockdown partially reversed ox-LDL-induced phenotypic changes, leading to increased SMA expression and decreased CD68 and MMP9 expression. In addition, ORO staining, BODIPY 493/503 staining, and Dil-ox-LDL uptake assays demonstrated that CDCP1 knockdown reduced intracellular lipid accumulation, lipid droplet formation, and ox-LDL uptake in mVSMCs. These findings suggest that

CDCP1 promotes macrophage-like phenotypic transition and lipid loading in mVSMCs under ox-LDL stimulation.

To investigate the downstream mechanism through which CDCP1 modulates VSMC phenotypic transition, RNA-seq was performed in mVSMCs after CDCP1 silencing. Analysis of differential expression identified 20 DEGs following CDCP1 knockdown, and subsequent KEGG enrichment analysis highlighting their prominent enrichment in the PI3K/AKT pathway. This finding suggested that PI3K/AKT signaling might participate in CDCP1-mediated regulation of pathological VSMC remodeling. Among DEGs associated with this pathway, ITGB4 caught our interest because it serves as an important upstream regulator of PI3K/AKT signaling and was markedly downregulated after CDCP1 knockdown.

To validate the bioinformatics findings, we further examined the expression of I proteins associated with the ITGB4/PI3K/AKT pathway in the aortic arch tissues of AS mouse. Immunofluorescence staining showed that ITGB4, p-PI3K, and p-AKT were elevated in aortic arch plaques from HFD-fed ApoE$^{-/-}$ mice, suggesting that the ITGB4/PI3K/AKT pathway was activated in atherosclerotic lesions. ITGB4, a type I transmembrane glycoprotein, belongs to the integrin family and participates in cell adhesion to the extracellular matrix and in intracellular signaling [24]. Previous research has demonstrated that ITGB4 can trigger downstream AKT signaling by interacting with the p85 regulatory subunit of PI3K through its intracellular domain[25]. The PI3K/AKT pathway is critical in AS development and VSMC phenotypic remodeling[26]. For instance, TRIM65 facilitates the progression of AS by inducing the transformation of VSMCs from a contractile to a synthetic phenotype via the activation of the PI3K/AKT/mTOR pathway[27]. In contrast, lncRNA HULC has been shown to alleviate aortic intimal injury and inhibit AS plaque development by inhibiting PI3K/AKT signaling[28]. Our *in vitro* results, consistent with these studies, indicated that ox-LDL stimulation elevated ITGB4 expression and enhanced PI3K and AKT phosphorylation in mVSMCs, whereas CDCP1 knockdown attenuated these changes. The results suggest that CDCP1 might facilitate the phenotypic transition of VSMCs triggered by ox-LDL through activating ITGB4/PI3K/AKT pathway.

Next, we explored how CDCP1 regulates ITGB4 expression. qPCR analysis showed that CDCP1 knockdown significantly reduced ITGB4 mRNA levels in mVSMCs, suggesting that CDCP1 may regulate ITGB4 expression at the transcriptional or post-transcriptional level. Because mRNA abundance is determined by both transcriptional activity and mRNA stability, we further examined ITGB4 promoter activity through a dual-luciferase reporter assay. The findings revealed that CDCP1 knockdown had no obvious effect on ITGB4 promoter activity, indicating that the reduction in ITGB4 expression was unlikely to be caused by transcriptional inhibition. In contrast, actinomycin D assays demonstrated that CDCP1 knockdown accelerated ITGB4 mRNA degradation and shortened its half-life. Notably, CHX chase assays showed that CDCP1 knockdown did not significantly alter the degradation rate of ITGB4 protein. These findings suggest that CDCP1 maintains ITGB4 expression mainly by enhancing ITGB4 mRNA stability, rather than by promoting ITGB4 transcription or suppressing ITGB4 protein degradation.

Rescue experiments provided additional validation for the involvement of the ITGB4/PI3K/AKT pathway in CDCP1-mediated regulation of mVSMCs phenotypic transition and lipid accumulation. Under CDCP1 knockdown and ox-LDL stimulation, ITGB4 overexpression or IGF-1 treatment enhanced intracellular lipid accumulation, lipid droplet formation, and ox-LDL uptake. Together, these results suggest that CDCP1 promotes macrophage-like phenotypic transition and lipid accumulation in mVSMCs by maintaining ITGB4 expression and activating the downstream PI3K/AKT pathway.

Nevertheless, several limitations need to be acknowledged. Firstly, although CDCP1 expression was increased in both human plaque datasets and mouse AS lesions, further validation in larger patient cohorts and plaque samples is necessary to determine its clinical relevance. Second, the present study mainly relied on CDCP1 knockdown *in vitro*; therefore, VSMC-specific CDCP1 knockout or overexpression models *in vivo* would be valuable for confirming its causal role in AS progression. Third, although our data indicate that CDCP1 regulates ITGB4 mRNA stability, the precise non-coding RNAs, RNA-binding proteins, or post-transcriptional regulatory mechanisms involved remain to be identified. Finally, AS is a complicated disease that involves endothelial cells, macrophages, immune cells, and VSMCs. Thus, the potential role of CDCP1 in other vascular or inflammatory cell types requires additional study.

The findings of this study suggest that CDCP1 is increased in AS plaques and contributes to the macrophage-like phenotypic transition and lipid accumulation in VSMCs triggered by ox-LDL. Mechanistically, CDCP1 maintains ITGB4 expression by enhancing ITGB4 mRNA stability, thereby triggers the PI3K/AKT pathway. These findings expand the understanding of CDCP1 function in vascular biology and imply that targeting the CDCP1 could serve as a potential approach for interfering with AS progression.

Declarations

1.Funding

This work was supported by the Shenzhen Science and Technology Program [JCYJ20250604125159002] and the Shenzhen Nanshan District Health Major Project [NSZD2024069].

2.Competing Interests

The authors have no relevant financial or non-financial interests to disclose.The authors declare that they have no competing interests.

3.Author Contributions

All authors contributed to the study conception and design. Material preparation, data collection and analysis were performed by Wanqiu Li, Bo Yuan and Huaihai Lu. Software, visualization, validation, investigation were performed by Wei Luo, Ling Li, Hanzhao Li, Ning Zhou and Jianglang Yuan. Resources, funding acquisition, supervision and project administration were performed by Qianqian Dong and Xin Ji.

The first draft of the manuscript was written by Wanqiu Li and all authors commented on previous versions of the manuscript. All authors read and approved the final manuscript.

4.Data Availability

The data that support the findings of this study are available from the corresponding author upon reasonable request.

5.Ethics approval

This study approved by the Experimental Animal Ethics Committee of Guangdong Medical Experimental Animal Center (number D202403-51), China. Futhermore, all animal experiments complied with the Guide for the Care and Use of Laboratory Animals (National Institutes of Health Publication No. 85-23, revised in 1996) and were reported following the Animal Research Report of In Vivo Experiments (ARRIVE) guidelines. This study does not involve clinical trials.

6.Patient consent for publication

Not applicable.This study did not involve human participants, data, specimens, or tissue.

7.Acknowledgment

The authors are grateful to all the experts who gave them guidance in experiments. This work was supported by the Shenzhen Science and Technology Program [JCYJ20250604125159002] and the Shenzhen Nanshan District Health Major Project [NSZD2024069].

References

1. Baek KI, Ryu K (2024) Role of Flow-Sensitive Endothelial Genes in Atherosclerosis and Antiatherogenic Therapeutics Development. J Cardiovasc Transl Res 17:609–623. https://doi.org/10.1007/s12265-023-10463-w
2. Nitz K, Herrmann J, Lerman A, Lutgens E (2024) Costimulatory and Coinhibitory Immune Checkpoints in Atherosclerosis: Therapeutic Targets in Atherosclerosis? JACC Basic Transl Sci 9:827–843. https://doi.org/10.1016/j.jacbts.2023.12.007
3. Wang K, Yin Z, Zhang Y, Wu X, Fan L (2025) From Bench to Clinic: Advances in Anti-Inflammatory Therapies for Atherosclerotic Coronary Artery Disease. FASEB J 39:e71056. https://doi.org/10.1096/fj.202502269R
4. Huang Y-C, Tsai Y-H, Lin L-C, Weng H-H, Lee J-D, Yang J-T (2024) Preliminary results on temporal evolution and clinical implications of atherosclerotic plaque in branch atheromatous disease after statin treatment. Ther Adv Neurol Disord 17:17562864241273902. https://doi.org/10.1177/17562864241273902

5. Yao J, Cai L, Chen Y, Zhang J, Zhuang W, Liang J, Li H (2022) Exosomes: mediators regulating the phenotypic transition of vascular smooth muscle cells in atherosclerosis. Cell Commun Signal 20:153. https://doi.org/10.1186/s12964-022-00949-6
6. Zhao L, Zhao L, Liu D, Huang F, Peng Q, Lu J, Zhou J, Zheng S, Liu X (2025) Vascular Smooth Muscle Cells: A Therapeutic Target in Atherosclerosis. Rev Cardiovasc Med 26:28240. https://doi.org/10.31083/RCM28240
7. Yurdagul A (2022) Crosstalk Between Macrophages and Vascular Smooth Muscle Cells in Atherosclerotic Plaque Stability. Arterioscler Thromb Vasc Biol 42:372–380. https://doi.org/10.1161/ATVBAHA.121.316233
8. Lambert J, Jørgensen HF (2025) Epigenetic regulation of vascular smooth muscle cell phenotypes in atherosclerosis. Atherosclerosis 401:119085. https://doi.org/10.1016/j.atherosclerosis.2024.119085
9. Cao G, Xuan X, Li Y, Hu J, Zhang R, Jin H, Dong H (2023) Single-cell RNA sequencing reveals the vascular smooth muscle cell phenotypic landscape in aortic aneurysm. Cell Commun Signal 21:113. https://doi.org/10.1186/s12964-023-01120-5
10. Qi X, Gao J, Li Z, Zhang G, Li J, Fu Y, Cai M, Wang H, Tong T (2022) CDCP1: A promising diagnostic biomarker and therapeutic target for human cancer. Life Sci 301:120600. https://doi.org/10.1016/j.lfs.2022.120600
11. Liu Y, Ma L, Zhu T, Wu D, Liu Y (2026) Extracellular vesicle-derived CDCP1 promotes chemoresistance and macrophage polarization in breast cancer. Hum Cell 39:65. https://doi.org/10.1007/s13577-026-01371-7
12. Oliveras T, Revuelta-López E, García-García C, Cserkóová A, Rueda F, Labata C, Ferrer M, Montero S, El-Ouaddi N, Martínez MJ, Roura S, Gálvez-Montón C (2022) Bayes-Genis, Circulating virome and inflammatory proteome in patients with ST-elevation myocardial infarction and primary ventricular fibrillation. Sci Rep 12:7910. https://doi.org/10.1038/s41598-022-12075-x
13. Ji X, Wang X, Dong Q, Li W, Zhou N, Yue X, Zhao D, Yang X (2025) CDCP1 knockdown suppresses PDGFRβ/AKT pathway-mediated vascular smooth muscle cell proliferation by inhibiting PDGFRβ endocytosis. PeerJ 13:e19114. https://doi.org/10.7717/peerj.19114
14. Zhang S, Bei Y, Huang Y, Huang Y, Hou L, Zheng X-L, Xu Y, Wu S, Dai X (2022) Induction of ferroptosis promotes vascular smooth muscle cell phenotypic switching and aggravates neointimal hyperplasia in mice. Mol Med 28:121. https://doi.org/10.1186/s10020-022-00549-7
15. Azar P, Jarr K-U, Gomez D, Jørgensen HF, Leeper NJ, Bochaton-Piallat M-L (2025) Smooth muscle cells in atherosclerosis: essential but overlooked translational perspectives. Eur Heart J 46:4862–4875. https://doi.org/10.1093/eurheartj/ehaf337
16. Song J, Cao C, Wang Z, Li H, Yang L, Kang J, Meng H, Li L, Liu J (2024) Mechanistic insights into the regression of atherosclerotic plaques. Front Physiol 15:1473709. https://doi.org/10.3389/fphys.2024.1473709

17. Fernández-Ruiz I (2022) Statins promote efferocytosis in atherosclerotic plaques. Nat Rev Cardiol 19:286. https://doi.org/10.1038/s41569-022-00699-5
18. Saponaro M, Flottmann S, Eckstein M, Hommerding O, Klümper N, Corvino D, Hosni S, Schmidt A, Mönig N, Schmidt D, Ellinger J, Toma M, Kristiansen G, Bald T, Alimonti A, Ritter M, Hölzel M, Alajati A (2023) CDCP1 expression is frequently increased in aggressive urothelial carcinoma and promotes urothelial tumor progression. Sci Rep 13:73. https://doi.org/10.1038/s41598-022-26579-z
19. Pollan SG, Huang F, Sperger JM, Lang JM, Morrissey C, Cress AE, Chu CY, Bhowmick NA, You S, Freeman MR, Spassov DS, Moasser MM, Carter WG, Satapathy SR, Shah K, Knudsen BS (2018) Regulation of inside-out β1-integrin activation by CDCP1, Oncogene 37 2817–2836. https://doi.org/10.1038/s41388-018-0142-2
20. Liu D, Wang M, Murthy V, McNamara DM, Nguyen TTL, Philips TJ, Vyas H, Gao H, Sahni J, Starling RC, Cooper LT, Skime MK, Batzler A, Jenkins GD, Barlera S, Pileggi S, Mestroni L, Merlo M, Sinagra G, Pinet F, Krejčí J, Chaloupka A, Miller JD, de Groote P, Tschumperlin DJ, Weinshilboum RM, Pereira NL (2023) Myocardial Recovery in Recent Onset Dilated Cardiomyopathy: Role of CDCP1 and Cardiac Fibrosis. Circ Res 133:810–825. https://doi.org/10.1161/CIRCRESAHA.123.323200
21. Zhao Y, Wang Z, Chen Y, Feng M, Liu X, Chen H, Wang N, Wang Z, Cao S, Ren J, Liu X, Zhao Y, Zhang Y (2024) Asprosin aggravates atherosclerosis via regulating the phenotype transformation of vascular smooth muscle cells. Int J Biol Macromol 268:131868. https://doi.org/10.1016/j.ijbiomac.2024.131868
22. Chin DD, Poon C, Wang J, Joo J, Ong V, Jiang Z, Cheng K, Plotkin A, Magee GA, Chung EJ (2021) miR-145 micelles mitigate atherosclerosis by modulating vascular smooth muscle cell phenotype. Biomaterials 273:120810. https://doi.org/10.1016/j.biomaterials.2021.120810
23. Shi X, Zhang Y, Han J, Peng W, Fang Z, Qin Y, Xu X, Lin J, Xiao F, Zhao L, Lin Y (2021) Tryptanthrin Regulates Vascular Smooth Muscle Cell Phenotypic Switching in Atherosclerosis by AMP-Activated Protein Kinase/Acetyl-CoA Carboxylase Signaling Pathway. J Cardiovasc Pharmacol 77:642–649. https://doi.org/10.1097/FJC.0000000000001008
24. Huang G, Zhou M, Lu D, Li J, Tang Q, Xiong C, Liang F, Chen R (2024) The mechanism of ITGB4 in tumor migration and invasion. Front Oncol 14:1421902. https://doi.org/10.3389/fonc.2024.1421902
25. Tong S, Wu J, Song Y, Fu W, Yuan Y, Zhong P, Liu Y, Wang B (2024) IDH1-mutant metabolite D-2-hydroxyglutarate inhibits proliferation and sensitizes glioma to temozolomide via down-regulating ITGB4/PI3K/AKT. Cell Death Discov 10:317. https://doi.org/10.1038/s41420-024-02088-y
26. Zhu L, Chen Q, Wang B, Fu J, Liu Z, Cui Y, Zhang R, Liu F, Niu S, Zhou Y (2026) PI3K/AKT signaling pathway: new strategies for treating atherosclerosis with plant-derived compounds. Front Pharmacol 17:1722493. https://doi.org/10.3389/fphar.2026.1722493
27. Zhou Z-X, Ma X-F, Xiong W-H, Ren Z, Jiang M, Deng N-H, Zhou B-B, Liu H-T, Zhou K, Hu H-J, Tang H-F, Zheng H, Jiang Z-S (2024) TRIM65 promotes vascular smooth muscle cell phenotypic transformation by activating PI3K/Akt/mTOR signaling during atherogenesis. Atherosclerosis 390:117430. https://doi.org/10.1016/j.atherosclerosis.2023.117430

28. Mu D, Li D, Li J, Yu H, Chen W, Liang J, Wang D, Li A, Qing Z, Zhang B (2021) Long non-coding RNA HULC protects against atherosclerosis via inhibition of PI3K/AKT signaling pathway. IUBMB Life 73:202–212. https://doi.org/10.1002/iub.2417

Figures

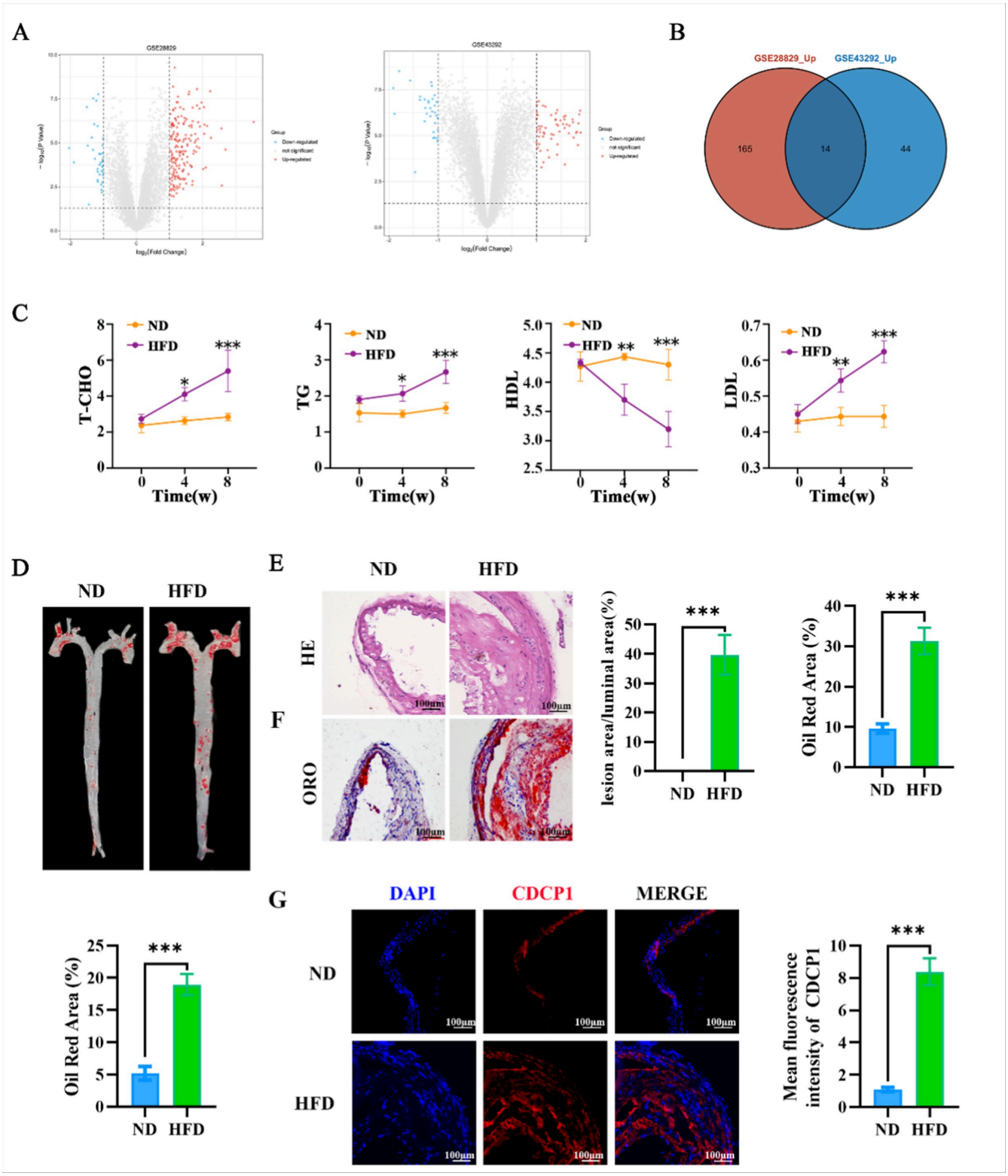


Figure 1

CDCP1 is highly expressed in AS mouse aortic arch tissues (A) Volcano plots showing DEGs in GSE43292 and GSE28829 datasets. (B) Venn diagram showing the overlapping DEGs among two GEO datasets. (C) Serum TC, TG, HDL-C, and LDL-C levels in each group of mice. (D) Representative ORO staining images of full-length aortas from each group. (E) Representative HE staining images of aortic arches from each group. (F) Representative ORO staining images of aortic arches from each group; (G) Representative immunohistochemical staining images and quantitative analysis of CDCP1 in aortic arch tissues from each group. *P<0.05, **P<0.01, ***P<0.001.

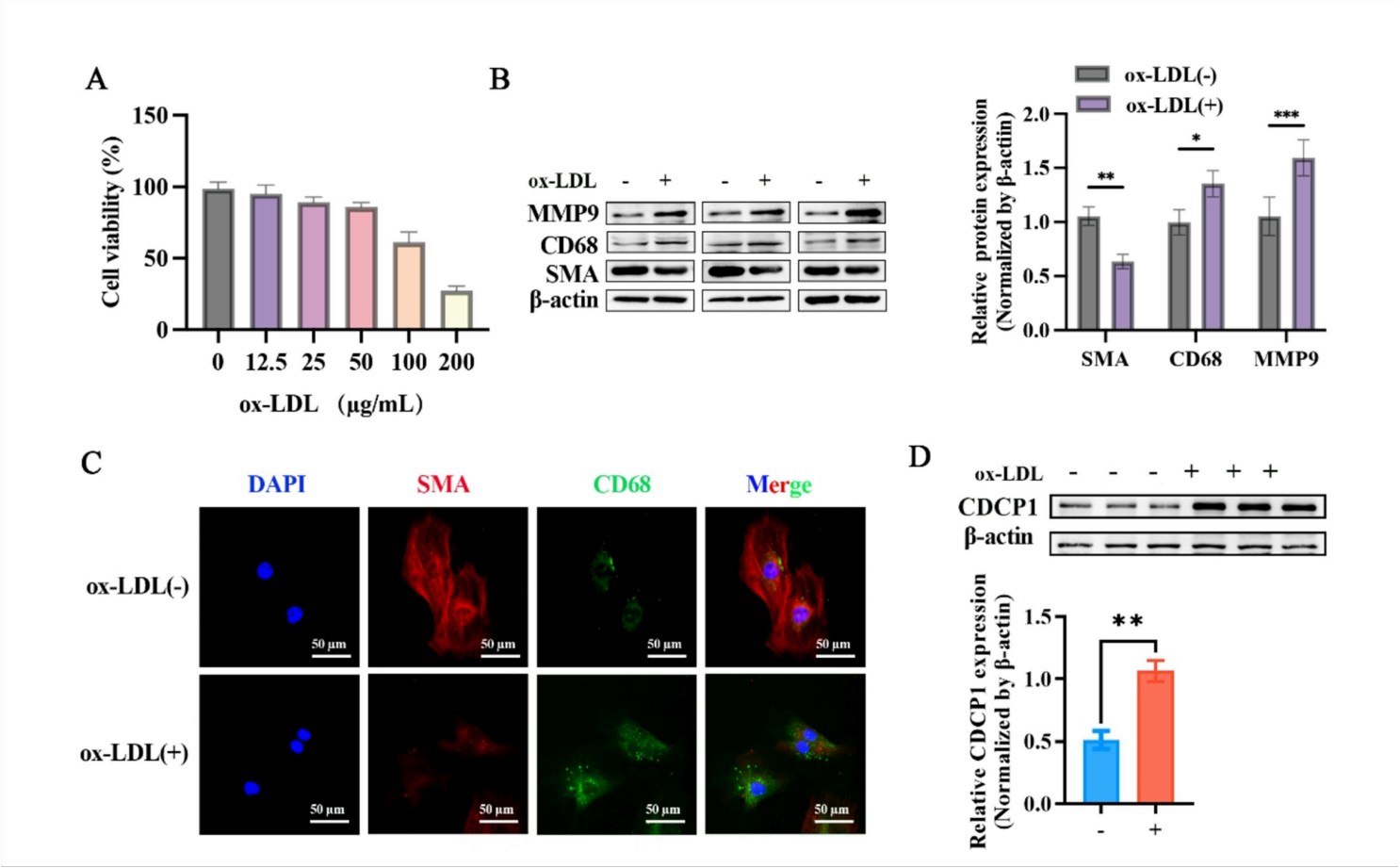


Figure 2

ox-LDL induces the macrophage-like phenotypic transition of mVSMCs and upregulates CDCP1 expression (A) CCK-8 assay evaluating the viability of mVSMCs exposed to various concentrations of ox-LDL. (B) Western blot analysis of SMA, CD68, and MMP9 protein expression in mVSMCs. (C) Immunofluorescence analysis of SMA and CD68 positive staining in mVSMCs. (D) Western blot analysis of CDCP1 protein expression in mVSMCs. *P<0.05, **P<0.01, ***P<0.001.

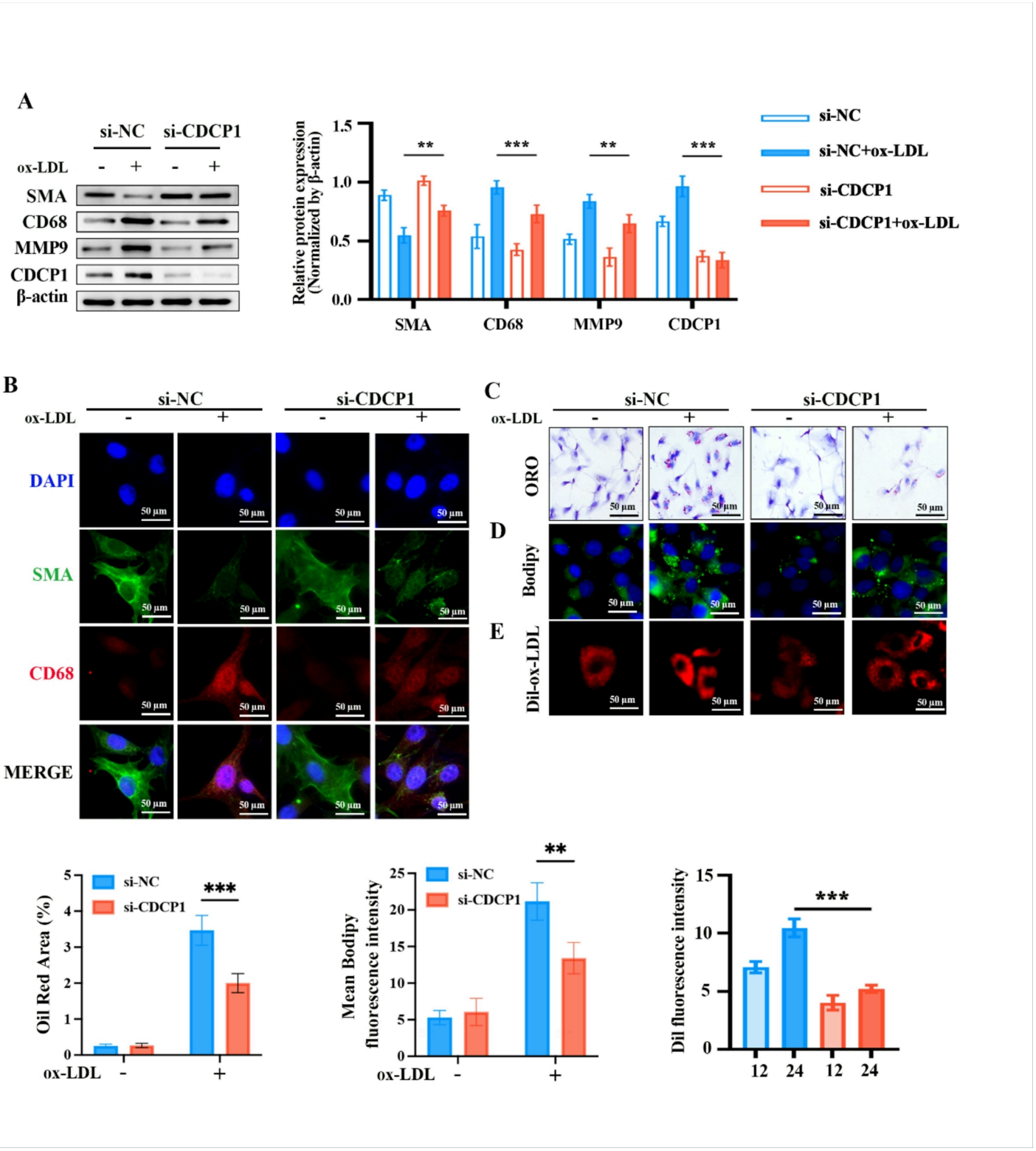


Figure 3

CDCP1 knockdown inhibits ox-LDL-induced macrophage-like phenotypic transition and lipid accumulation in mVSMCs (A) Western blot analysis of CDCP1, SMA, CD68, and MMP9 protein expression in mVSMCs across different treatment groups. (B) Immunofluorescence analysis of SMA and CD68 positive staining in mVSMCs across different treatment groups. (C) ORO staining assessing lipid

accumulation in mVSMCs. (D) BODIPY 493/503 staining assessing lipid droplet formation in mVSMCs. (E) Dil-ox-LDL staining assessing ox-LDL uptake in mVSMCs. *P< 0.05, **P < 0.01, ***P < 0.001.

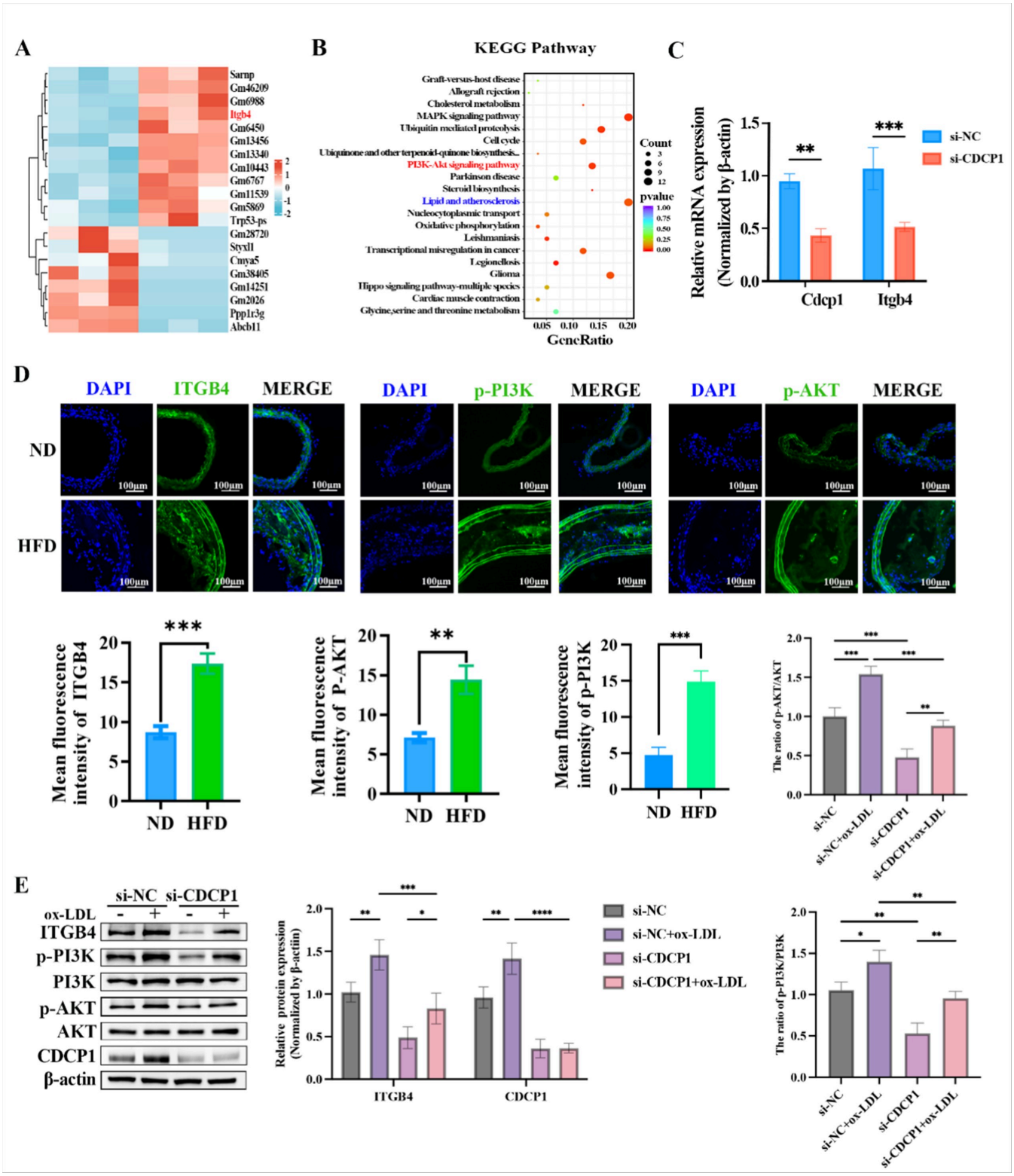


Figure 4

Knocking down CDCP1 *in vitro* suppresses the activation of the ITGB4/PI3K/AKT pathway (A) Heatmap displaying 20 DEGs between the si-NC and si-CDCP1 groups. (B) The analysis of KEGG pathway

enrichment reveals the top 20 pathways with significant enrichment for DEGs. (C) qPCR analysis of ITGB4 mRNA expression in si-NC and si-CDCP1 groups of mVSMCs. (D) Immunofluorescence analysis of ITGB4, p-PI3K, and p-AKT in the aortic arch tissues of mice. (E) Western blot analysis of ITGB4, p-PI3K, PI3K, p-AKT, and AKT protein levels in mVSMCs across different treatment groups. *P < 0.05, **P < 0.01, ***P < 0.001.

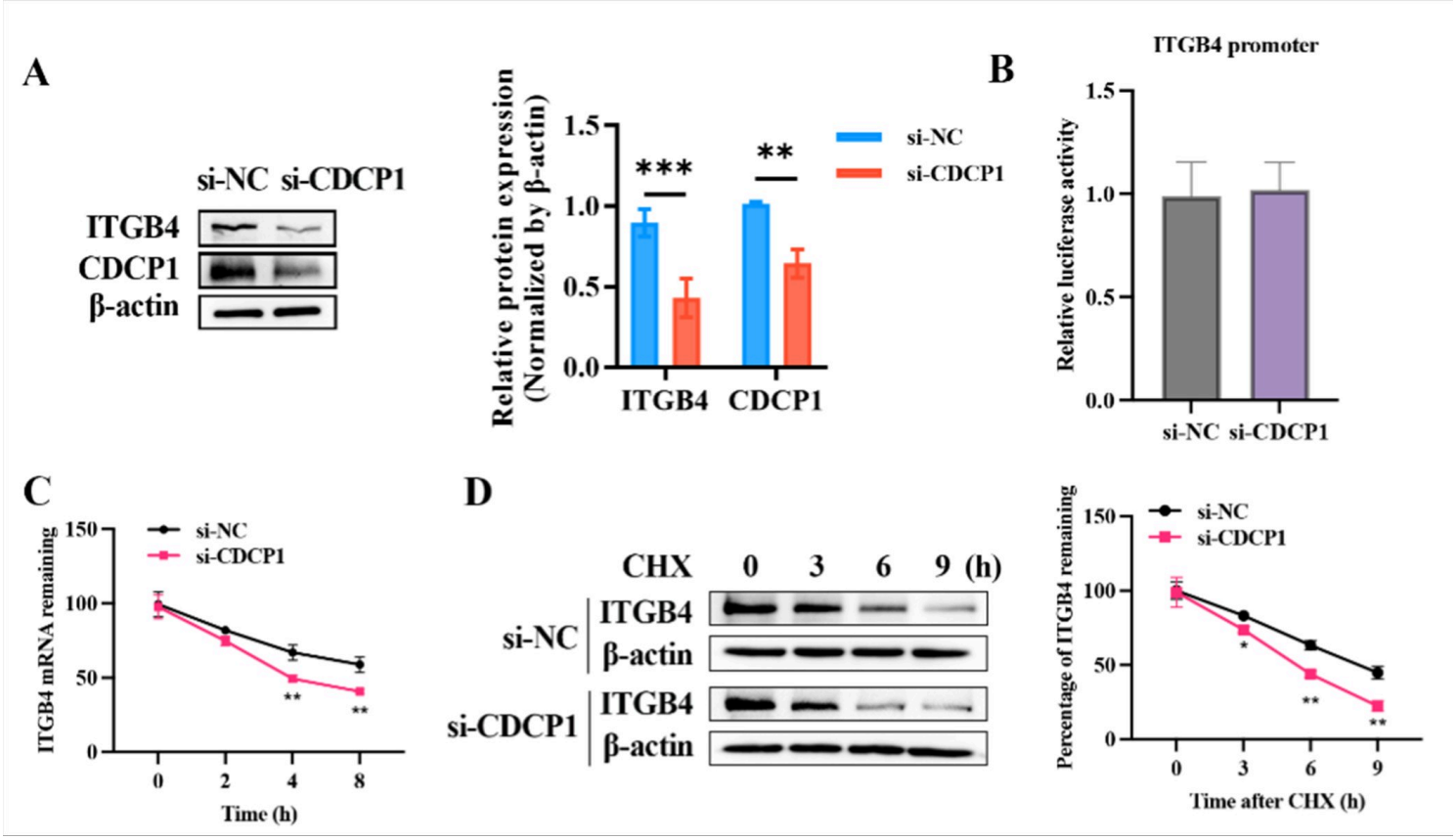


Figure 5

CDCP1 knockdown reduces ITGB4 expression by decreasing ITGB4 mRNA stability (A) Western blot analysis of ITGB4 protein expression in si-NC and si-CDCP1 groups of mVSMCs. (B) Dual-luciferase reporter assay assessing changes in ITGB4 promoter activity following CDCP1 knockdown. (C) Assessment of ITGB4 mRNA degradation in si-NC and si-CDCP1 groups of mVSMCs following actinomycin D treatment. (D) CHX chase assay assessing ITGB4 protein stability. *P< 0.05, **P < 0.01, ***P < 0.001.

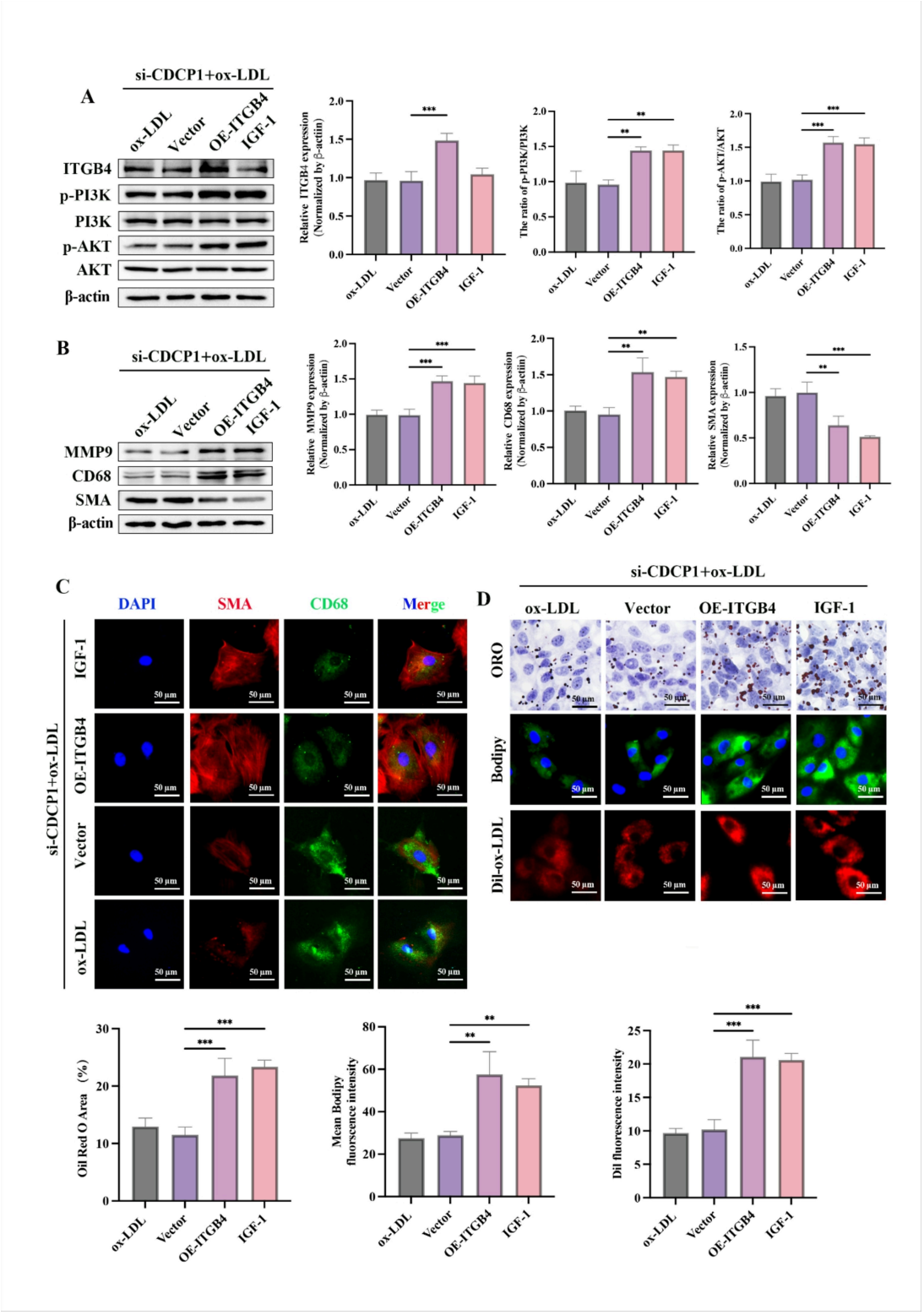


Figure 6

CDCP1 promotes the macrophage-like phenotypic transition and lipid accumulation in mVSMCs via the ITGB4/PI3K/AKT pathway (A) Western blot analysis of ITGB4, p-PI3K, PI3K, p-AKT, and AKT levels in mVSMCs across different treatment groups. (B) Western blot analysis of SMA, CD68, and MMP9 levels in mVSMCs across different treatment groups. (C) Immunofluorescence analysis of SMA and CD68 positive staining in mVSMCs across different treatment groups. (D) ORO staining assessing lipid

accumulation in mVSMCs. (E) BODIPY 493/503 staining assessing lipid droplet formation in mVSMCs. (F) Dil-ox-LDL staining assessing ox-LDL uptake in mVSMCs. *P < 0.05, **P < 0.01, ***P < 0.001.